Title

Surface force measurements and simulations of mussel-derived peptide adhesives on wet organic surfaces.

Journal

Proceedings of the National Academy of Sciences of the United States of America, 113(16)

ISSN

0027-8424

Authors

Levine, Zachary A
Rapp, Michael V
Wei, Wei
et al.

Publication Date

2016-04-01

DOI

10.1073/pnas.1603065113

Peer reviewed

Surface force measurements and simulations of mussel-derived peptide adhesives on wet organic surfaces

Zachary A. Levine[a,b,1], Michael V. Rapp[c,1], Wei Wei[d], Ryan Gotchy Mullen[c], Chun Wu[e], Gül H. Zerze[f], Jeetain Mittal[f], J. Herbert Waite[d,g], Jacob N. Israelachvili[c,d,2], and Joan-Emma Shea[a,b,2]

[a]Department of Physics, University of California, Santa Barbara, CA 93106; [b]Department of Chemistry and Biochemistry, University of California, Santa Barbara, CA 93106; [c]Department of Chemical Engineering, University of California, Santa Barbara, CA 93106; [d]Materials Research Laboratory, University of California, Santa Barbara, CA 93106; [e]Department of Chemistry and Biochemistry, Rowan University, Glassboro, NJ 08028; [f]Department of Chemical and Biomolecular Engineering, Lehigh University, Bethlehem, PA 18015; and [g]Department of Molecular, Cell and Developmental Biology, University of California, Santa Barbara, CA 93106

Contributed by Jacob N. Israelachvili, February 25, 2016 (sent for review December 11, 2015; reviewed by Deborah E. Leckband and Jim Pfaendtner)

Translating sticky biological molecules—such as mussel foot proteins (MFPs)—into synthetic, cost-effective underwater adhesives with adjustable nano- and macroscale characteristics requires an intimate understanding of the glue's molecular interactions. To help facilitate the next generation of aqueous adhesives, we performed a combination of surface forces apparatus (SFA) measurements and replica-exchange molecular dynamics (REMD) simulations on a synthetic, easy to prepare, Dopa-containing peptide (MFP-3s peptide), which adheres to organic surfaces just as effectively as its wild-type protein analog. Experiments and simulations both show significant differences in peptide adsorption on CH_3-terminated (hydrophobic) and OH-terminated (hydrophilic) self-assembled monolayers (SAMs), where adsorption is strongest on hydrophobic SAMs because of orientationally specific interactions with Dopa. Additional umbrella-sampling simulations yield free-energy profiles that quantitatively agree with SFA measurements and are used to extract the adhesive properties of individual amino acids within the context of MFP-3s peptide adhesion, revealing a delicate balance between van der Waals, hydrophobic, and electrostatic forces.

mussel foot proteins | self-assembled monolayers | protein folding | molecular dynamics simulations | surface forces apparatus

Demand for biologically inspired underwater adhesives, such as those secreted by marine mussels to adhere to a wide variety of hard and soft surfaces (1), have seen tremendous growth over the past decade, with applications to bone sealing (2), dental and medical transplants (3), coronary artery coatings (4), cell encapsulants (5), and other systems. To facilitate the construction of next-generation underwater adhesives, we can mimic existing biological glues—such as those containing mussel foot proteins (MFPs)—and translate the glues' structures to create biologically inspired synthetic adhesives (6). Doing so requires detailed knowledge of the molecular interactions that take place, many of which occur on length and time scales that are, at present, too small to be accurately characterized by experiments. Therefore, more sophisticated studies that combine theoretical modeling with state-of-the-art experiments are necessary for advancing the development of novel underwater adhesives.

Although the mussel's talent for wet adhesion has been known for centuries, the true molecular understanding of adhesion began in 1952 with Brown's hypothesis that the mussel's byssus thread and adhesive plaques are comprised of intrinsically disordered proteins rich in the catecholic amino acid dopa (Dopa) (7). With knowledge of Dopa's binding ability, an abundance of Dopa-containing polymers were synthesized that displayed impressive adhesive (8, 9), coating (1, 4), structural (10, 11), and self-healing (12, 13) properties. The surface forces apparatus (SFA) has been used to measure the adhesion of MFP-containing glues (1, 6, 14–17); however, it remains difficult to unambiguously identify individual or cooperative interactions of amino acids that facilitate adhesion because few theoretical models are available for comparison (18, 19).

The majority of MFP-inspired adhesives have been investigated on pristine surfaces in solution (18–22); however, under more realistic conditions, surfaces targeted for adhesion are rarely free from contaminants and are fouled with organic films that impede robust adhesion. Yu et al. (17) demonstrated that certain MFPs promote strong adhesion to hydrophobic self-assembled monolayers (SAMs), presumably through direct interactions with the surface, while exhibiting weak adhesion to hydrophilic SAMs.

Here, we study a peptide mimic of the full-length 45-residue MFP-3s protein (23) (termed MFP-3s peptide), which consists of only 25 residues (sequence: N-GYDGYNWPYGYNGYRYGWN KGWNGY-C). The peptide (shown in Fig. 1) retains 7 out of 11 Dopa (denoted here as Y) and 3 out of 4 tryptophan (W) residues found in the full-length protein, in addition to 3 charged residues, which play a dominant role in the adhesion of MFPs to hydrophobic and hydrophilic organic surfaces (17). Short, MFP-derived peptides such as the MFP-3s peptide are overwhelmingly appealing alternatives to full proteins (6) because (*i*) the shorter length allows more tractable theoretical and experimental analysis

Significance

The need for bio-inspired wet adhesives has significantly increased in the past few decades (e.g., for dental and medical transplants, coronary artery coatings, cell encapsulants, etc.). However, the molecular basis behind catechol-facilitated adhesion to organic surfaces remains unclear, thus hindering synthesis and optimization of novel underwater adhesives. The present combined experimental and theoretical study reconciles bioadhesion measurements of novel catechol-containing peptides to self-assembled monolayers (SAMs) with all-atom molecular dynamics simulations, yielding a comprehensive framework that explicitly identifies the basis for underwater adhesion. Simulations and surface forces apparatus measurements agree with one another, and both approaches show strong peptide adhesion to hydrophobic SAMs, and weak peptide adhesion to hydrophilic SAMs, providing a starting point for the development of next-generation underwater glues.

Author contributions: Z.A.L., M.V.R., J.H.W., J.N.I., and J.-E.S. designed research; Z.A.L. and M.V.R. performed research; W.W., R.G.M., C.W., G.H.Z., and J.M. contributed new reagents/analytic tools; Z.A.L., M.V.R., J.H.W., J.N.I., and J.-E.S. analyzed data; and Z.A.L., M.V.R., J.H.W., J.N.I., and J.-E.S. wrote the paper.

Reviewers: D.E.L., University of Illinois; and J.P., University of Washington.

The authors declare no conflict of interest.

[1]Z.A.L. and M.V.R. contributed equally to this work.

[2]To whom correspondence may be addressed. Email: jacob@engineering.ucsb.edu or shea@chem.ucsb.edu.

This article contains supporting information online at www.pnas.org/lookup/suppl/doi:10.1073/pnas.1603065113/-/DCSupplemental.

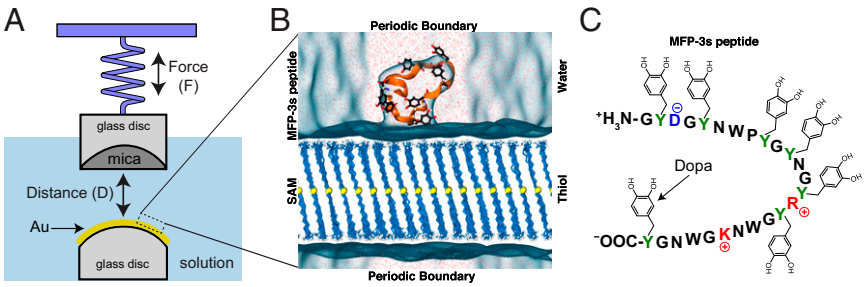

Fig. 1. (*A*) Schematic of the mica and gold surfaces used in SFA measurements. CH_3 or OH self-assembled monolayers are adsorbed onto the gold surface. (*B*) Configuration of a typical MD simulation containing an MFP-3s peptide and a self-assembled monolayer. (*C*) Amino acid sequence for the MFP-3s peptide containing Dopa (posttranslationally modified from tyrosine).

of surface interactions, (*ii*) peptides are significantly cheaper and easier to produce compared with extracting and purifying biological proteins, and (*iii*) Dopa-containing peptides can be engineered and optimized to retain or enhance the adhesive properties of full-length proteins. We show, using a combination of SFA measurements and molecular dynamics (MD) simulations, that MFP-3s peptides exhibit strong binding to organic hydrophobic (CH_3-terminated) surfaces through direct, catechol-mediated interactions with surface methyl groups, where the underlying mechanisms of adhesion are elucidated. Alternatively, these peptides exhibit weak binding affinities to hydrophilic (OH-terminated) surfaces. Results from both experiments and simulations show excellent agreement with one another.

Results and Discussion

Peptides Strongly Adhere to Hydrophobic But Not Hydrophilic Underwater Interfaces. Using the SFA (Fig. 2), we determined the interaction force (F) as a function of distance (D) between mica (with radius R) and either a CH_3-terminated (hydrophobic) SAM surface or an OH-terminated (hydrophilic) SAM surface in a solution of MFP-3s peptide. In agreement with our previous full-length MFP measurements on SAMs (17), MFP-3s peptides exhibit strong adhesion forces between hydrophobic surfaces and moderate-to-weak adhesion forces between hydrophilic surfaces. Firstly, SAMs were adsorbed onto smooth (rms roughness 0.2 nm) gold surfaces and then mounted in the SFA opposite from a mica surface. Control force–distance measurements between mica and the SAMs are shown in Fig. S1. In each experiment, increasing aliquots of MFP-3s peptides were injected between the two surfaces before force measurements were performed, until the surfaces were saturated with bound peptides. At saturation, the surfaces are fully covered with a single layer of peptide. Further injection of the peptide beyond the saturation point resulted in both a decrease in adhesion and an increase in the peptide film thickness (Fig. S2), attributable to stacking of multiple peptide layers. Using the Johnson–Kendall–Roberts theory (24) for adhering surfaces, the measured interaction force per unit radius is converted into an adhesion energy per unit area ($E_{ad} = F_{ad}/1.5\pi R$). The average adhesion energy required to separate a peptide film from a hydrophobic and hydrophilic SAM (E_{ad}) was -7.7 ± 1.9 and -0.4 ± 0.3 mJ/m^2, respectively. Energy minima for each system were observed at distances (r_{min}) of 2.5 ± 0.2 and 2.7 ± 0.3 nm from the gold SFA surface for hydrophobic and hydrophilic systems.

To gain further insight into the adhesion mechanisms of this peptide, we performed umbrella-sampling simulations to estimate free energy (or potential of mean force) as a function of distance (25). PMF simulations yielded 1D free-energy profiles of MFP-3s peptide adhesion as a function of the peptide's center-of-mass distance from the SAM substrate, where attractive and repulsive regions can be seen in Fig. 3. These results show a large -34.7 kT energy minimum for the peptide at 1.9 nm above the hydrophobic SAM. In contrast, the peptide is only bound with -6.2 kT of energy on hydrophilic SAMs at an equilibrium distance (r_{min}) of 2.1 nm, almost six times weaker than on hydrophobic surfaces. These energies were then converted to an adhesion per unit area (Fig. 3, secondary axis) by dividing the adhesion energy by the average peptide contact area of about 8–9 nm^2. The simulated adhesion strengths for the MFP-3s peptide on hydrophobic and hydrophilic SAMs were 15.9 and 2.9 mJ/m^2, respectively.

If we compare the ratios of the energy minima (at r_{min}) between simulations (Fig. 3) and experiments (E_{ad}) (Fig. 2), we find that on hydrophobic SAMs, $E_{sim}/E_{exp} = (-15.9 \text{ mJ/m}^2)/(-7.7 \text{ mJ/m}^2) = 2.1$, and on hydrophilic SAMs, $(-2.9 \text{ mJ/m}^2)/(-0.4 \text{ mJ/m}^2) = 7.2$. These ratios are approximate and are subject to change if the SFA error bars are strictly applied; however, adhesion from the simulations was always stronger than what was measured in experiments. Simulations exhibit increased peptide adhesion because only one surface is present, where all adhering residues must detach for separation to occur. However, in SFA experiments there are two opposing surfaces, and peptides can remain bound to the upper mica surface as the mica separates from the opposing SAM surface. On average, if symmetric adhesion occurs on the SFA, where half the Dopa residues bind to opposite surfaces, we would expect to measure approximately half the adhesive force in SFA experiments compared with simulations. However, if nonsymmetrical binding of Dopa to lower SAM surfaces (compared with upper mica surfaces) occurs, this discrepancy can vary considerably, as observed on hydrophilic surfaces. Despite these factors, both methods agree that MFP-3s peptides bind more weakly to, and at slightly further distances from, OH-terminated SAMs.

Overall, the experimental and computational measurements are in good agreement with one another. In the simulations, the peptide's distance is measured from the SAM substrate to the peptide center-of-mass. In the SFA experiments, distance is measured from the SAM substrate to the opposing mica surface. The length of the SAMs' alkane chains in both experiment and simulation were also the same. Therefore, we obtain a similar r_{min} by offsetting the simulated value by the peptide's radius of gyration (R_g), which was around 0.8 nm (Fig. 4). From simulations, we find that $(r_{min} + R_g) = 2.7$ nm on hydrophobic SAMs and 2.9 nm on hydrophilic SAMs, precisely within the uncertainty observed in SFA experiments (2.5 ± 0.2 and 2.7 ± 0.3 nm, respectively). Even the difference in r_{min} between hydrophobic and hydrophilic surfaces (0.2 nm) was accurately reproduced in the simulations.

DOPA Binds Parallel to Hydrophobic Organic Interfaces and Perpendicular to Hydrophilic Organic Interfaces. At crystalline oxide or mineral surfaces—such as mica or TiO_2—MFPs adhere in solution via coordination or bidentate bonds with Dopa's hydroxyls and electrostatic interactions with charged residues (26, 27). However, at organic surfaces with varying polarities and thermally mobile surface groups, the adhesive interactions are expected to differ. To probe the atomic binding behaviors and orientations of MFP-3s peptides to the two surfaces, we performed replica-exchange MD (REMD) simulations, as described in *Methods*. Fig. 4 highlights the most dominant peptide conformations found from REMD on each surface, where Dopa tends to be oriented parallel (≤45° from the plane of the surface)

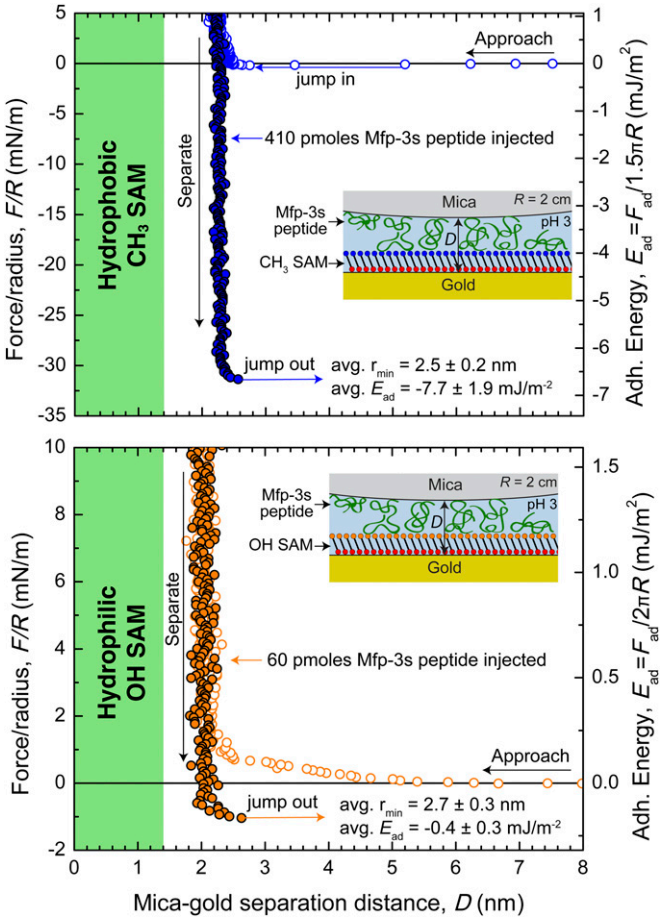

Fig. 2. Representative force–distance profiles for MFP-3s peptides adsorbed at full saturation between either a hydrophobic CH_3-SAM film (*Upper*) or a hydrophilic OH-SAM film (*Lower*) and mica, in a solution of 0.1 M acetic acid and 0.25 M KNO_3 (pH 3). Data points on approach are shown as open circles, whereas data points measured during separation are shown as closed circles. (*Inset*) Schematic diagram of the interacting surfaces.

near hydrophobic SAMs and perpendicular (>45° from the plane of the surface) near hydrophilic SAMs. This observation confirms our earlier hypothesis (17) that Dopa will take on parallel and perpendicular orientations on hydrophobic and hydrophilic surfaces, respectively. In contrast to the bidentate interactions observed at crystalline surfaces, only monodentate hydrogen bonds were observed between Dopa and the thermally mobile OH-SAM surface. The bond lifetimes of monodentate interactions are significantly shorter than bidentate interactions, which dramatically reduces the peptide's adhesion to the OH-SAM surface compared with mineral or oxide surfaces. These results also reveal that Dopa, which is amphiphilic, sometimes orients outward toward the bulk solution with its hydroxyls hydrated, whereas tryptophan (which is purely hydrophobic) orients toward the hydrophobic interior of the peptide's globular core. Peptide secondary structures are also highlighted in Fig. 4, where hydrophobic SAMs promote extended, flatter conformations, whereas hydrophilic surfaces reinforce more globular bulk states, similar to other small proteins on organic surfaces (28). Detailed secondary structural information is presented in Fig. S3 as a function of the peptide's amino acid sequence, where a small but noticeable increase in β-bridging occurs on the surface of hydrophobic SAMs. However, because the MFP-3s peptide is intrinsically disordered, no major secondary structures persist.

Hydrophobic Surfaces Unfold MFP-3s Peptides, Whereas Hydrophilic Surfaces Stabilize MFP-3s Peptides. From simulations, we extract the top three MFP-3s peptide conformations found in bulk solution and on hydrophobic and hydrophilic SAMs (Fig. 4, *Left*). We find that whereas the peptide spends little time in any single conformation (where every cluster persists ≤6% of the total simulation time), the top three dominant structures (labeled clusters a, b, and c in Fig. 4) exhibit similar morphologies. These trends were not limited to the top three peptide conformations, as can be seen in Fig. S4. However, for clarity, only the top three peptide clusters are presented in detail, because the remaining structures were variants of the first three conformations. To better characterize the energetics of peptide folding, we plot complimentary 2D free-energy surfaces (FES) to the right of each set (Fig. 4, *Right*), as a function of the peptide's end-to-end distance (R_{ee}) and radius of gyration (R_g). In bulk water, MFP-3s peptides can traverse across multiple FES minima by increasing their end-to-end distance from 0.5 to 2 nm; however, this movement always occurs at constant R_g (0.8 nm). Higher R_g are only accessible to MFP-3s peptides under energy penalties of 5–7 kT; however, surfaces significantly modify these barriers. For clarity, each cluster is explicitly identified on the FES, typically residing at free-energy minima.

On hydrophobic and hydrophilic SAMs, peptide adhesion is observed in all three of the most dominant peptide clusters, where Dopa facilitates peptide binding in parallel and perpendicular orientations on CH_3- and OH-terminated SAMs, respectively. Additional free-energy basins appear near hydrophobic SAMs, where MFP-3s peptides take on either comparable (0.8 nm) or larger (1.1 nm) radii of gyration compared with bulk. Similarly, larger end-to-end distances are observed near hydrophobic SAMs (up to 3.2 nm, as shown in clusters a and c), but these states are separated from other states (e.g., cluster b) by about 6 kT. However, peptides may change their radii of gyration (through extension or contraction) without leaving the SAM surface, as shown in Fig. 4, *Far Upper Right*. Conversely, hydrophilic surfaces stabilize bulk peptide conformations, although peptides remain bound to the surface by polar interactions between the interface and Dopa hydroxyls. The reduction in the number of free-energy basins near hydrophilic SAMs is also striking, with peptides primarily taking on compact (small R_{ee}, small R_g) conformations near the SAM surface. Multiple end-to-end peptide distances are also observed on hydrophilic SAMs, although clusters a and c are only separated from cluster b by about 2–3 kT, because of the persistence of the bulk state.

We also observed a decrease in the number of intramolecular hydrogen bonds formed between MFP-3s peptide backbones (C=O and N-H groups) near hydrophobic SAM surfaces. Fig. S5 shows the emergence of a number of new peptide structures on hydrophobic surfaces that contain very few hydrogen bonds, thereby reinforcing more extended peptide conformations with high-contact surface

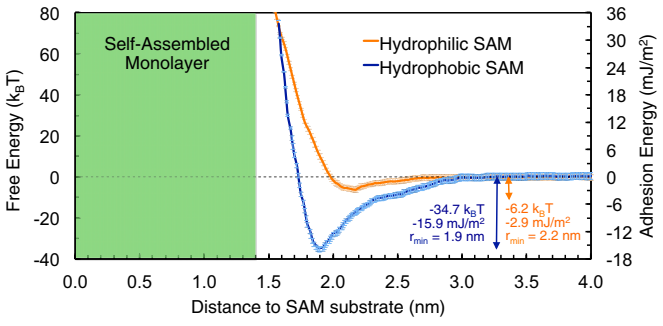

Fig. 3. Simulated potentials of mean force for the MFP-3s peptide on organic surfaces, plotted as a function of distance from the SAM substrate. Free energies (primary axis) are also converted to adhesion energies per unit area (secondary axis) by dividing by the peptide's convergent contact area with the surface (on the order of 9 nm^2). Peptides strongly adhere to hydrophobic SAMs (blue) and weakly to hydrophilic SAMs (orange).

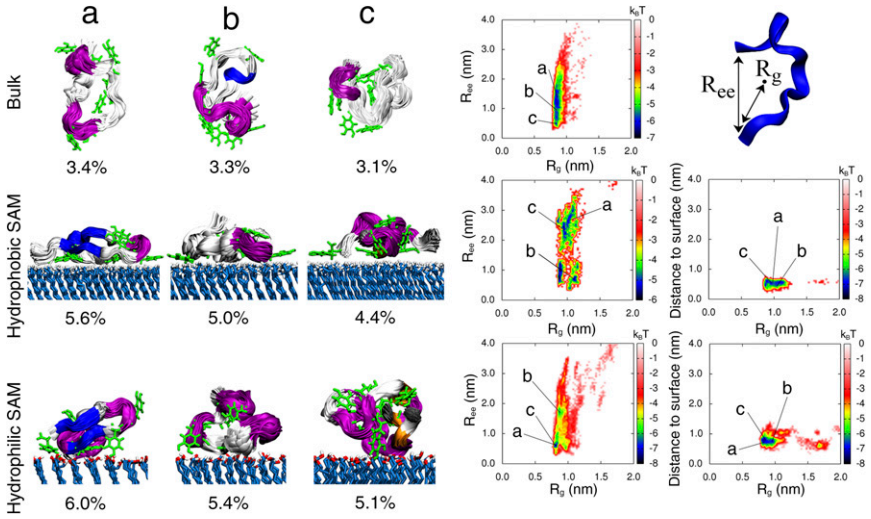

Fig. 4. Top three dominant MFP-3s peptide morphologies (clusters a–c) are shown in the bulk or on SAM surfaces (*Left*), grouped in descending order, with corresponding percentages of time spent in each configuration. Free-energy landscapes for each of these systems are also displayed (*Right*), as a function of the peptide end-to-end distance (R_{ee}) and radius of gyration (R_g). Favorable low-energy basins are in black and blue, whereas less-favorable energy states are in red and white.

areas. Hydrophilic surfaces, however, do not strongly perturb the distribution of peptide hydrogen bonds from bulk, thereby encouraging peptide conformations with smaller surface contact areas.

A number of Arg-Asp salt bridges are also observed in MFP-3s peptides on the surface of hydrophobic SAMs. Fig. S6 shows multiple FES plotted as a function of the proximities between charged Asp, Arg, and Lys residues, in addition to the residues' positions relative to the SAM surface. Energy minima at small distances (e.g., ≤0.3 nm) indicate strong electrostatic interactions between oppositely charged residues. Asp-Arg salt bridges persist on hydrophobic SAMs, although Lys-Asp salt brides are not often observed because Lys favors the SAM surface instead, despite the reduction of hydrating water molecules at the interface. On hydrophilic SAMs, both Arg-Asp and Lys-Asp salt bridges are observed, although Lys and Arg maintain contact with the OH SAM surface. Interestingly, Arg is bound so tightly to Asp that it sometimes pulls the negatively charged residue with it upon binding to the surface.

We also plot FES for individual Dopa and Trp residues in the MFP-3s peptide (Fig. S7), to extract the per-residue energetics of Dopa/Trp rotation at organic interfaces, as a function of the residues' distances to the surface. We observed that almost all Dopa residues were oriented perpendicular (90°) to organic surfaces far above the interface (or in random orientations that averaged to 90°) but subsequently rotated parallel (0° or 180°) on hydrophobic surfaces during approach. The energy required for Dopa to transition from perpendicular to parallel orientations ranges from 4 to 4.5 kT; however, Trp is more freely able to rotate on hydrophobic organic surfaces with an energy penalty of only 1–2 kT. Results were quite different on hydrophilic surfaces, where multiple Dopa and Trp orientations were observed close to 45° from the surface.

Nearby Charged Amino Acids Enhance DOPA Adhesion to Organic Surfaces. Whereas Dopa residues clearly contribute to robust adhesion in MFPs, there are other amino acids (such as Lys) that can perturb the conformations of Dopa. To better understand the chemical context between Dopa and adjacent charged residues, and what roles they play in binding to organic surfaces, we performed umbrella-sampling simulations, where we used either a single-capped Dopa residue (Fig. 5), a single-capped Lys residue (Fig. S8, *Upper*), or a combined Dopa-Gly-Lys peptide (Fig. S8, *Lower*) for each SAM surface. This technique allowed for the decomposition and subsequent identification of adhesive contributions from individual amino acids, while also providing information about their bound conformations. Lys was selected as a complimentary amino acid because it was recently shown to enhance Dopa adhesion (29), but the molecular mechanisms behind this behavior are highly contested. Fig. 5 shows the free-energy profile for Dopa, where multiple interesting features stand out. When Dopa settles at hydrophilic r_{min}, it binds to OH-terminated SAMs at a somewhat tilted (~45°) angle, where Dopa's hydroxyl and peripheral hydrogens bind to the negatively charged SAM hydroxyl oxygens. This orientation is also observed during MFP-3s peptide binding, where multiple Dopa residues were tilted on hydrophilic surfaces (Fig. S7). Per unit area, Dopa was over 4.5 times more adhesive to hydrophobic surfaces compared with the entire MFP-3s peptide and 11.6 times more adhesive to hydrophilic surfaces than the MFP-3s peptide. Similarly, Lys was over 10 times more adhesive per unit area on hydrophilic surfaces compared with the MFP-3s peptide (attributable primarily to Lys′s positive electrostatic attraction to the surface, which extends far into bulk) and was also 1.7 times more adhesive on hydrophobic SAMs compared with the MFP-3s peptide. Near hydrophobic SAMs, the charged Lys terminus is hydrated in bulk water; however, the alkyl chain remains inside the hydrophobic region near the interface. When Dopa and Lys were combined in a model tripeptide (Fig. S8, *Lower*), adhesion to surfaces was cooperative, where peptide free energies on both hydrophobic and hydrophilic surfaces remained attractive out to 3.5 nm (further into bulk than any of the individual amino acids).

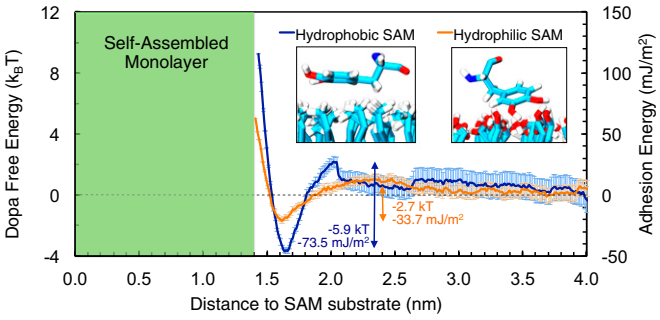

Fig. 5. Simulated potentials of mean force for a single Dopa residue on a hydrophobic and hydrophilic SAM. Inset images show the typical conformations observed for Dopa at energy-minimized locations (r_{min}).

Therefore, whereas Dopa is a better adhesive (per unit area) on hydrophobic surfaces, and Lys a better adhesive (per unit area) on hydrophilic surfaces, adjacent Dopa- and Lys-containing molecules (29) are better overall adhesives on a wide variety of organic surfaces because of the adjacent Dopa- and Lys-containing molecules' concerted binding motifs.

By using theoretical models of peptide adhesion, which highlight the nanoscale interactions between Dopa and organic surfaces, and by validating these models with SFA measurements, we have taken important first steps in revealing the atomic mechanisms behind Dopa adhesion. These results successfully bridge atomistic theories of Dopa adsorption to macroscale material measurements of novel peptides on a wide-variety of wet organic surfaces, thereby enabling future studies to synthesize and optimize stronger, next-generation underwater adhesives.

These results (highlighted in Fig. 6) also validate earlier theoretical hypothesis (17) about the preferred orientations of Dopa on hydrophobic and hydrophilic organic surfaces and have far-reaching implications regarding the mechanism of MFP adhesion to generalized organic surfaces, including cellular membranes. We have demonstrated that interfacial solvation is inextricably tied to the peptide's adhesive performance: at the fluctuating, vapor-like CH_3/water interface (30), hydrophobic association mediates strong peptide adhesion, whereas at the hydrophilic OH/water interface, the competition between water and the peptide for hydrogen bonds to the surface drastically reduces the overall adhesion. By better understanding how biological surfaces stabilize or destabilize intrinsically disordered proteins (31), and by using unique amphiphilic residues that modulate adhesion to these surfaces, we have provided a template for more sophisticated studies that seek to optimize next-generation bioadhesives under a number of unique biological conditions.

Methods

Simulation Structures. Self-assembled monolayers were constructed by creating a fixed 2D grid of sulfur atoms in a diamond geometry in the middle of a unit cell (30). Then, a 10-atom alkane chain $(CH_2)_{10}$ was attached to both the top and bottom of each sulfur anchor, terminated by either a CH_3 group (for hydrophobic interfaces) or an OH group (for hydrophilic interfaces). SAM chains were left unfrozen to observe if fluctuations in surface spacing would promote bidentate bonding between MFP dopa residues and surface groups. Parameterization of SAMs were performed by Garde et al. (30). The net charge of each SAM was kept neutral. Box dimensions were on the order of $8 \times 8 \times 10$ nm^3, and periodic boundary conditions were implemented to mitigate system size effects and reduce computation. The system was then hydrated at room temperature with a semiisotropic barostat that froze the XY box dimensions, whereas the Z dimension was allowed to fluctuate to establish 1 bar of pressure. An unfolded MFP-3s peptide (with +1e net charge) was then added to the bulk solution above the SAM, alongside a chloride counter ion. The Z box dimension was subsequently fixed after bulk water density was reestablished at 1 bar of pressure in Z, where the system was ready to be simulated under a canonical (constant volume) ensemble.

REMD Simulations. Simulations were carried out using GROMACS 4.6.1 (32) on the Stampede supercomputer at the Texas Advanced Computing Cluster. REMD (33) simulations consisted of 70 replicas at increasingly higher temperatures that (after a number of preliminary values were tested) yielded an average exchange rate of 25% between adjacent replicas during the initial 10 ns, ranging in temperature from 288 to 506 K. Exchanges between replicas were attempted every 3 ps to allow an adequate mixing of states to occur. Replicas were initially heated for 20 ns, followed by a 200-ns production run at constant temperature; however, only the final 100 ns was analyzed and summarized here. Peptide topologies were derived from the AMBER03* force field (30, 34, 35). Partial charges for dopa residues (Dopa) were parameterized by fitting quantum gas-phase potentials of each atom using the restrained electrostatic potential (RESP) method (36), whereas other parameters (bond, angle, torsion, and Lennard–Jones constants) were taken from AMBER03*. The use of idealized Lennard–Jones and Coulomb potentials in simulations allowed for the reproduction of a number of interactions between molecules such as van der Waals forces, dispersion, hydrogen-bonding, hydrophobicity, and dielectric responses. Although more complex Hamiltonians can be implemented in MD that incorporate additional terms, the Hamiltonian in the AMBER03* force field is sufficient for capturing the most dominant molecular interactions. TIP3P rigid water molecules (37) were used to hydrate each system, where up to 15000 explicit water molecules were used per simulation box. Simulations were initially equilibrated with a weakly coupled, semi-isotropic Berendsen barostat (38) at 1 bar, with an isothermal compressibility of 4.5×10^{-5} bar^{-1}, and a velocity-rescaled thermostat (39) that maintained temperature at 300 K. After the box-dimensions converged, the unit-cell volume was fixed, and switched over to a canonical NVT ensemble under a Nosé-Hoover thermostat (40) for the remainder of the study. A leapfrog algorithm was used to integrate Newton's equations of motion with an integration time step of 2 fs. Peptide and SAM molecular bonds were constrained using the LINCS algorithm (41), while water bonds were constrained using the SETTLE algorithm (42). Short-range electrostatic and Lennard–Jones forces were truncated at 1 nm, where long-range interactions took over using a Particle Mesh Ewald (PME) algorithm (43).

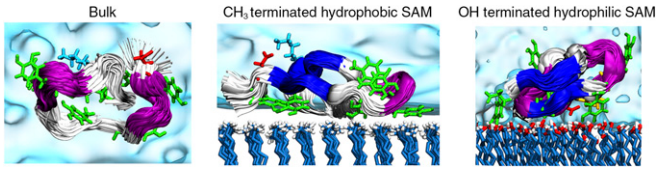

Fig. 6. Snapshot of the most dominant peptide morphologies found in bulk and on organic surfaces. Dark blue peptide backbones indicate β-strands, whereas purple backbones indicate turn regions. Green aromatic residues represent Dopa, red and cyan residues represent aspartic acid and arginine, and white and red interfacial atoms represent hydrogen and oxygen atoms, respectively. Water is depicted as a bright blue surface that hydrates each system uniquely.

Adhesive Force Calculations. Additional simulations were carried out to ascertain the potentials of mean force (PMF) on MFP-3s peptides, Dopa, Lys, and Dopa-Gly-Lys peptides on hydrophobic and hydrophilic SAMs. PMFs were extracted by umbrella sampling (25) molecules along a reaction coordinate normal to the SAM surface (in 1 Å bins) for a total of 10 ns per bin. A spring with a constant of 8,000 kJ mol^{-1} nm^{-2} was used to sample each reaction coordinate, and the weighted histogram analysis method (WHAM) (25) was used to extract free-energy profiles from normalized probability measurements. Bayesian bootstrapping was used (in conjunction with WHAM) to generate PMF error bars.

Simulation Analysis and Tools. Molecular graphics were generated with Visual Molecular Dynamics (VMD) 1.9.1 (44). The GROMACS tools g_hbond, g_traj, g_gyration, and g_cluster were used to measure the probabilities of intramolecular hydrogen bonding, peptide end-to-end distance (R_{ee}), the radius of gyration (R_g), and clusters of dominant peptide morphologies at room temperature. Hydrogen bonds were defined with an O-H spacing of 0.25 nm or smaller and O-H-N angles of 30° or less. R_{ee} was measured from the N-Gly center of mass to the C-Dopa center of mass. MFP-3s peptide conformations were clustered according to the criteria of Daura et al. (45), which compares protein backbones (excluding terminal amino acids) and groups them together based on a root mean square cutoff of 0.14 nm or less. Secondary structures were extracted using the DSSP tool (46).

MFP-3s Peptide Synthesis. Peptides were commercially synthesized using solid-phase peptide synthesis (GenScript). Tyr residues in the peptides were then hydroxylated in-house to Dopa by using commercially available mushroom tyrosinase (Sigma Aldrich), where the yield of Dopa conversion was controlled by fine-tuning the enzyme/substrate ratios and reaction times. The resulting MFP-3s peptides contained, on average, seven Dopa units per molecule, which was confirmed by amino acid analysis and mass spectrometry.

SAM Surface Preparation. Self-assembled CH_3 and OH monolayers were prepared on molecularly smooth gold surfaces using a previously described technique (17, 47). First, a 45-nm layer of gold was deposited onto a freshly cleaved mica surface using electron beam deposition. Individual pieces of gold-coated mica were glued, with the gold side down, onto cylindrical glass SFA discs [radius (R), ~2 cm] using a UV-curable adhesive. After the glue had set, the discs were immersed in ethanol, and the mica back-sheets were carefully peeled away from the underlying gold layers. The templating procedure results in cylindrically shaped and molecularly smooth gold surfaces with 0.2-nm rms roughness. After cleaving, the pristine gold surfaces were immersed in 1 mM solutions of either 1-undecanethiol (CH_3-SAM) (Sigma Aldrich)

or 11-mercapto-1-undecanol (OH-SAM) (Sigma Aldrich) in ethanol for 18 h to adsorb the respective monolayer. Following the adsorption, the surfaces were rinsed with ethanol for 30 s to remove excess SAM molecules, dried under N_2, and installed in the SFA for force measurements.

SFA. SFA measurements were performed with a SFA 2000 (SurForce), and the full details of the SFA technique may be found elsewhere (48). Briefly, a freshly cleaved, back-silvered mica surface was glued to a cylindrical glass disk and installed in the SFA with the mica surface facing the SAM surface. Droplets of pH 3 buffer solution (0.1 M acetic acid plus 0.25 M KNO_3; Sigma Aldrich) were injected into the gap between the mica and SAM surfaces (~50 μL total volume), and force measurements were performed between the surfaces in buffer solution. Picomolar amounts of MFP-3s peptide—suspended in the same buffer solution—were then injected into the gap solution between the two surfaces and allowed to adsorb and equilibrate for 30 min. Force measurements were then performed between the surfaces at an approach/separation rate of ~1 nm/s, with the interactions mediated by the adsorbed layers of MFP-3s peptide. The absolute separation distance between the two surfaces was measured with fringes of equal chromatic order (FECO) assuming a two-layer interferometer between the gold and silver layers (49, 50). After multiple force measurements were performed and found to be reproducible with a given amount of injected peptide, an additional picomolar aliquot of MFP-3s peptide was injected between surfaces. The peptides were again allowed to adsorb for 30 min, where additional force measurements were performed. Within a single experiment, this process was repeated until the adhesion between the surfaces either plateaued or began to decrease with greater amounts of injected MFP-3s peptide. The force measurements presented in this work are representative of at least four separate experimental setups for each SAM type.

ACKNOWLEDGMENTS. The authors acknowledge the Texas Advanced Computing Center (TACC) at The University of Texas at Austin for providing high performance computing resources that have contributed to the research results reported in this paper. Partial financial support was provided by National Science Foundation (NSF) Grant MCB-1158577. This work was also supported by the MRSEC Program of the NSF under Award DMR 1121053 and the Center for Scientific Computing at the UCSB California NanoSystems Institute (Grant CNS-0960316). M.V.R. acknowledges support from the NSF Graduate Research Fellowship Program. W.W. was supported in part by National Institutes of Health Grant R01 DE018468. Work at Lehigh University was supported by the US Department of Energy (DOE), Office of Science, Basic Energy Sciences (BES) under Award DE-SC0013979. This work used the Extreme Science and Engineering Discovery Environment (XSEDE) (TG-MCA05S027), which is supported by National Science Foundation Grant ACI-1053575.

1. Lee BP, Messersmith PB, Israelachvili JN, Waite JH (2011) Mussel-inspired adhesives and coatings. *Annu Rev Mater Res* 41:99–132.
2. Winslow BD, Shao H, Stewart RJ, Tresco PA (2010) Biocompatibility of adhesive complex coacervates modeled after the sandcastle glue of Phragmatopoma californica for craniofacial reconstruction. *Biomaterials* 31(36):9373–9381.
3. Long M, Rack HJ (1998) Titanium alloys in total joint replacement–A materials science perspective. *Biomaterials* 19(18):1621–1639.
4. Kastrup CJ, et al. (2012) Painting blood vessels and atherosclerotic plaques with an adhesive drug depot. *Proc Natl Acad Sci USA* 109(52):21444–21449.
5. Yang SH, et al. (2011) Mussel-inspired encapsulation and functionalization of individual yeast cells. *J Am Chem Soc* 133(9):2795–2797.
6. Wei W, et al. (2015) Bridging adhesion of mussel-inspired peptides: Role of charge, chain length, and surface type. *Langmuir* 31(3):1105–1112.
7. Brown CH (1952) Some structural proteins of Mytilus-Edulis. *Q J Microsc Sci* 93(4): 487–502.
8. Lee H, Dellatore SM, Miller WM, Messersmith PB (2007) Mussel-inspired surface chemistry for multifunctional coatings. *Science* 318(5849):426–430.
9. Shao H, Stewart RJ (2010) Biomimetic underwater adhesives with environmentally triggered setting mechanisms. *Adv Mater* 22(6):729–733.
10. Ryu J, Ku SH, Lee H, Park CB (2010) Mussel-inspired polydopamine coating as a universal route to hydroxyapatite crystallization. *Adv Funct Mater* 20(13):2132–2139.
11. Podsiadlo P, Liu ZQ, Paterson D, Messersmith PB, Kotov NA (2007) Fusion of seashell nacre and marine bioadhesive analogs: High-strength nanocompoisite by layer-by-layer assembly of clay and L-3,4-dihydroxyphenylalanine polymer. *Adv Mater* 19(7):949–955.
12. Krogsgaard M, Behrens MA, Pedersen JS, Birkedal H (2013) Self-healing mussel-inspired multi-pH-responsive hydrogels. *Biomacromolecules* 14(2):297–301.
13. Ahn BK, Lee DW, Israelachvili JN, Waite JH (2014) Surface-initiated self-healing of polymers in aqueous media. *Nat Mater* 13(9):867–872.
14. Lin Q, et al. (2007) Adhesion mechanisms of the mussel foot proteins mfp-1 and mfp-3. *Proc Natl Acad Sci USA* 104(10):3782–3786.
15. Yu J, et al. (2011) Mussel protein adhesion depends on interprotein thiol-mediated redox modulation. *Nat Chem Biol* 7(9):588–590.
16. Danner EW, Kan Y, Hammer MU, Israelachvili JN, Waite JH (2012) Adhesion of mussel foot protein Mefp-5 to mica: An underwater superglue. *Biochemistry* 51(33):6511–6518.
17. Yu J, et al. (2013) Adaptive hydrophobic and hydrophilic interactions of mussel foot proteins with organic thin films. *Proc Natl Acad Sci USA* 110(39):15680–15685.
18. Qin Z, Buehler MJ (2014) Molecular mechanics of mussel adhesion proteins. *J Mech Phys Solids* 62:19–30.
19. Qin Z, Buehler M (2012) Molecular mechanics of dihydroxyphenylalanine at a silica interface. *Appl Phys Lett* 101(8):083702.
20. Lin S, et al. (2014) Tuning heterogeneous poly(dopamine) structures and mechanics: In silico covalent cross-linking and thin film nanoindentation. *Soft Matter* 10(3):457–464.
21. Leng C, et al. (2013) Interfacial structure of a DOPA-inspired adhesive polymer studied by sum frequency generation vibrational spectroscopy. *Langmuir* 29(22):6659–6664.
22. Qin Z, Buehler MJ (2013) Impact tolerance in mussel thread networks by heterogeneous material distribution. *Nat Commun* 4:2187.
23. Wei W, et al. (2014) A mussel-derived one component adhesive coacervate. *Acta Biomater* 10(4):1663–1670.
24. Johnson K, Kendall K, Roberts A (1971) Surface energy and the contact of elastic solids. *Proc R Soc A: Math Phys Eng Sci* 324(1558)::301–313.
25. Souaille M, Roux B (2001) Extension to the weighted histogram analysis method: Combining umbrella sampling with free energy calculations. *Comput Phys Commun* 135(1):40–57.
26. Ye Q, Zhou F, Liu W (2011) Bioinspired catecholic chemistry for surface modification. *Chem Soc Rev* 40(7):4244–4258.
27. Kristoffersen HH, Shea J-E, Metiu H (2015) Catechol and HCl adsorption on TiO2(110) in vacuum and at the water-TiO2 interface. *J Phys Chem Lett* 6(12):2277–2281.
28. Levine ZA, Fischer SA, Shea J-E, Pfaendtner J (2015) Trp-cage folding on organic surfaces. *J Phys Chem B* 119(33):10417–10425.
29. Maier GP, Rapp MV, Waite JH, Israelachvili JN, Butler A (2015) BIOLOGICAL ADHESIVES. Adaptive synergy between catechol and lysine promotes wet adhesion by surface salt displacement. *Science* 349(6248):628–632.
30. Godawat R, Jamadagni SN, Garde S (2009) Characterizing hydrophobicity of interfaces by using cavity formation, solute binding, and water correlations. *Proc Natl Acad Sci USA* 106(36):15119–15124.
31. Miller CM, Brown AC, Mittal J (2014) Disorder in cholesterol-binding functionality of CRAC peptides: A molecular dynamics study. *J Phys Chem B* 118(46):13169–13174.
32. Hess B, Kutzner C, van der Spoel D, Lindahl E (2008) GROMACS 4: Algorithms for highly efficient, load-balanced, and scalable molecular simulation. *J Chem Theory Comput* 4(3):435–447.
33. Sugita Y, Okamoto Y (1999) Replica-exchange molecular dynamics method for protein folding. *Chem Phys Lett* 314(1-2):141–151.
34. Beauchamp KA, Lin Y-S, Das R, Pande VS (2012) Are protein force fields getting better? A systematic benchmark on 524 diverse NMR measurements. *J Chem Theory Comput* 8(4):1409–1414.
35. Wang J, Wolf RM, Caldwell JW, Kollman PA, Case DA (2004) Development and testing of a general amber force field. *J Comput Chem* 25(9):1157–1174.
36. Bayly CI, Cieplak P, Cornell W, Kollman PA (1993) A well-behaved electrostatic potential based method using charge restraints for deriving atomic charges: The RESP model. *J Phys Chem* 97(40):10269–10280.
37. Jorgensen WL, Chandrasekhar J, Madura JD, Impey RW, Klein ML (1983) Comparison of simple potential functions for simulating liquid water. *J Chem Phys* 79(2):926–935.
38. Berendsen HJC, Postma JPM, Vangunsteren WF, Dinola A, Haak JR (1984) Molecular-dynamics with coupling to an external bath. *J Chem Phys* 81(8):3684–3690.
39. Bussi G, Donadio D, Parrinello M (2007) Canonical sampling through velocity rescaling. *J Chem Phys* 126(1):014101.
40. Hoover WG (1985) Canonical dynamics: Equilibrium phase-space distributions. *Phys Rev A* 31(3):1695–1697.
41. Hess B, Bekker H, Berendsen HJC, Fraaije JGEM (1997) LINCS: A linear constraint solver for molecular simulations. *J Comput Chem* 18(12):1463–1472.
42. Miyamoto S, Kollman PA (1992) Settle - An analytical version of the shake and rattle algorithm for rigid water models. *J Comput Chem* 13(8):952–962.
43. Essmann U, et al. (1995) A smooth particle mesh Ewald method. *J Chem Phys* 103(19):8577–8593.
44. Humphrey W, Dalke A, Schulten K (1996) VMD: Visual molecular dynamics. *J Mol Graph* 14(1):33–38, 27–28.
45. Daura X, et al. (2001) The beta-peptide hairpin in solution: Conformational study of a beta-hexapeptide in methanol by NMR spectroscopy and MD simulation. *J Am Chem Soc* 123(10):2393–2404.
46. Kabsch W, Sander C (1983) Dictionary of protein secondary structure: Pattern recognition of hydrogen-bonded and geometrical features. *Biopolymers* 22(12):2577–2637.
47. Chai L, Klein J (2007) Large area, molecularly smooth (0.2 nm rms) gold films for surface forces and other studies. *Langmuir* 23(14):7777–7783.
48. Israelachvili J, et al. (2010) Recent advances in the surface forces apparatus (SFA) technique. *Rep Prog Phys* 73:036601.
49. Israelachvili J (1973) Optical studies of thin films. *J Coll Int Sci* 44:259–272.
50. Donaldson SH, Jr, et al. (2013) Asymmetric electrostatic and hydrophobic-hydrophilic interaction forces between mica surfaces and silicone polymer thin films. *ACS Nano* 7(11):10094–10104.